Composites: Part A 201 (2026) 109393

Contents lists available at ScienceDirect

Composites Part A

journal homepage: www.elsevier.com/locate/compositesa

Intrinsic self-healing of polyamide 6/carbon fiber thermoplastic laminates

Davide Perin [a,*], Giulia Fredi [a,*], Pietro Russo [b], Alessandro Pegoretti [a], Andrea Dorigato [a]

[a] University of Trento, Department of Industrial Engineering and INSTM Research Unit, Via Sommarive 9, 38123 Trento, Italy
[b] Institute for Polymers, Composites and Biomaterials, National Research Council, Via Campi Flegrei 34, 80078 Pozzuoli, NA, Italy

GRAPHICAL ABSTRACT

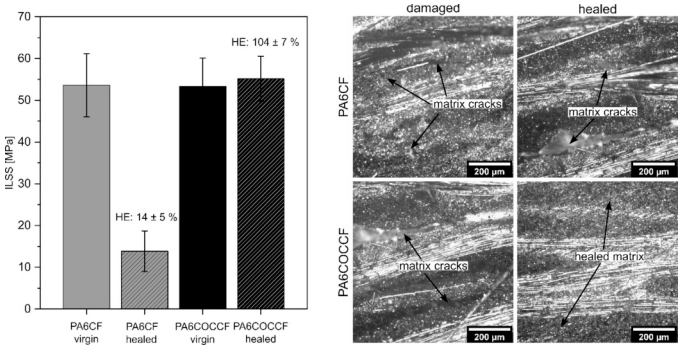

ARTICLE INFO

Keywords:
Self-healing
Thermoplastic composites
Polyamide 6
Cyclic olefinic copolymer
Interlaminar shear strength

ABSTRACT

This study investigates the self-healing capabilities of continuous carbon fiber (CF)-reinforced thermoplastic laminates, prepared via film stacking using an optimized polyamide 6 (PA6)/cyclic olefinic copolymer (COC)/ethylene glycidyl methacrylate (E-GMA) self-healing matrix (66.5/28.5/5 wt%) coupled with bidirectional CF fabrics. The self-healing composite demonstrates comparable porosity (2.3–2.7 vol%) to neat PA6/CF laminate (3.6–4.4 vol%) and exhibits enhanced tensile properties, with 43 % higher ultimate tensile strength (534 MPa vs. 374 MPa), likely due to improved fiber–matrix interaction through E-GMA compatibilization. However, the flexural strength decreases by 17 % (498 MPa vs. 599 MPa) for the self-healing system compared to the neat PA6/CF laminate, attributed to both the lower fiber volume fraction and the reduced tensile strength and stiffness of the PA6/COC/E-GMA matrix relative to neat PA6. The most significant finding is the exceptional self-healing performance, evaluated through short-beam shear (SBS) testing, which creates matrix-dominated damage while preserving fiber integrity. After thermal mending, the self-healing composite achieves complete damage restoration and full recovery of the interlaminar shear strength (ILSS), while neat PA6 composite shows minimal healing capability (14 %). Microstructural analysis confirms that the compatibilized COC effectively flows and fills the matrix cracks and delaminated regions during thermal mending. This work demonstrates for the first time the successful integration of intrinsic self-healing capabilities into continuous CF thermoplastic laminates below the matrix softening temperature by integrating intrinsically and thermally mendable

* Corresponding authors.
E-mail addresses: davide.perin-1@unitn.it (D. Perin), giulia.fredi@unitn.it (G. Fredi).

https://doi.org/10.1016/j.compositesa.2025.109393
Received 7 August 2025; Received in revised form 20 October 2025; Accepted 22 October 2025
Available online 25 October 2025
1359-835X/© 2025 The Author(s). Published by Elsevier Ltd. This is an open access article under the CC BY license (http://creativecommons.org/licenses/by/4.0/).

copolymers, thus providing a foundation for damage-tolerant structural applications where autonomous repair capabilities and extended service life are critical.

1. Introduction

Fiber-reinforced polymer composites (FRPCs) have become increasingly important in structural applications across the automotive, aerospace, and renewable energy sectors owing to their exceptional strength-to-weight ratio, corrosion resistance, and design flexibility [1]. However, a critical limitation of composite materials is their susceptibility to damage accumulation during their service life, including matrix cracking, delamination, and fiber breakage, which can significantly compromise structural integrity and lead to catastrophic failure [1,2]. Traditional repair methods are often costly and may require complete component replacement, raising economic and environmental concerns. A transformative approach to address these challenges is represented by self-healing composites: thanks to specific mechanisms that can repair microdamage, these materials offer the potential to reduce maintenance costs and improve reliability and safety, but also to extend component lifespan and reduce material waste, thereby contributing to sustainable material development [2,3].

Self-healing strategies can be categorized into two main types: extrinsic and intrinsic. Extrinsic systems incorporate microcapsules or hollow fibers that, upon damage, release reactive compounds that flow into cracks and cure or polymerize in situ [4–7]. Intrinsic types, on the other hand, utilize resources already embedded within the matrix, e.g., Diels-Alder reactions, reversible chemical bonds, or thermoplastic healing agents [8]. This last approach involves using, as a matrix, an immiscible blend in which the dispersed phase is a polymer with low softening (glass transition or melting) temperature, i.e., a healing agent. When damage occurs, the application of an external stimulus (e.g., heat, voltage, or magnetic field) causes these agents to soften and flow into the damaged areas, effectively repairing the cracks upon cooling [9,10]. This process can be repeated multiple times and does not require the use of expensive matrices or the inclusion of separate capsules or vascular networks, thereby simplifying manufacturing and reducing costs. Moreover, this approach has been also proven to be effective in repairing a damaged fiber/matrix interface [11,12].

Although the use of thermoplastic healing agents has been thoroughly investigated in thermosetting polymers [13–25], there is still a significant gap in understanding these processes in thermoplastic matrix composites. These materials are particularly intriguing from an engineering standpoint due to quicker production cycles and recyclability, which are becoming increasingly vital for sustainable material development [26–28]. Although thermoplastic composites are generally considered weldable and repairable [29], traditional repairing requires overcoming the melting/softening temperature of the matrix, but this can translate into reaching very high temperatures, especially for engineering thermoplastic polymers, and can lead to the distortion or the thermal affection of the whole part. Hence, introducing mechanisms enabling thermal mending at lower temperatures can be advantageous also for thermoplastic composites. In fact, this temperature reduction allows components to be repaired in-situ (rather than ex situ, as commonly done for thermoplastics) or with minimal fixturing, reduces energy consumption significantly, and decreases the likeliness of damaging surrounding materials or structures. Recently, our group concentrated on self-healing thermoplastic composites with a polyamide 6 (PA6) matrix and containing polycaprolactone (PCL) or cyclic olefin copolymer (COC) as healing agents [30–33]. Although various thermoplastic healing agents have been studied for self-healing purposes, COC stands out as a highly promising option because of its outstanding thermal stability, low glass transition temperature, and chemical compatibility with engineering thermoplastics when properly compatibilized.

Our previous investigations systematically optimized PA6/COC self-healing blends through comprehensive rheological, microstructural, and thermomechanical characterization. The incorporation of ethylene glycidyl methacrylate (E-GMA) as a compatibilizer proved crucial for optimizing the dispersion of COC and interfacial adhesion with PA6, significantly improving processability and healing efficiency [32]. The optimal formulation, comprising PA6 with 30 wt% COC and 5 wt% E-GMA, demonstrated healing efficiencies (evaluated as the ratio of the critical stress intensity factor (K_{IC}) of healed and virgin samples) of 38 % in the quasi-static mode and 82 % in the impact mode when subjected to thermal healing at 160 °C [32]. Furthermore, our recent work on discontinuous carbon fiber reinforced self-healing thermoplastic composites revealed remarkable potential for fatigue life extension, with healing processes improving fatigue performance by approx. 77 % through effective repair of matrix micro-damages and delamination [33].

Building on these developments in thermoplastic self-healing matrices, logical progression involves investigating their performance in continuous carbon-fiber-reinforced systems. However, the transition from discontinuous to continuous fiber reinforcement introduces several challenges. The processing of long-fiber thermoplastic composites typically requires different manufacturing approaches, such as film stacking followed by consolidation through hot pressing, which may significantly influence the self-healing mechanism effectiveness compared to injection-molded short-fiber systems. Film stacking requires the production of thin thermoplastic films containing a self-healing blend, which must maintain adequate processability and a homogeneous and finely dispersed healing agent distribution. In addition, the laminated structure created through film stacking may affect the mobility and flow of the healing agent during thermal mending. The presence of continuous fiber layers could potentially lead to an accumulation of the healing agent in the interlaminar region and hinder its migration to damage sites, or conversely, create preferential flow paths that enhance healing efficiency along fiber–matrix interfaces. This could produce different repair efficiencies depending on whether the damage is inter- or intralaminar. Moreover, the high viscosity of modified thermoplastic matrices could complicate fiber impregnation and the high processing temperatures required for engineering thermoplastics (>200 °C) can degrade many healing agents. These challenges, combined with the historical dominance of thermoset matrices in structural composites, have created a significant knowledge gap in the study of intrinsic self-healing in continuous fiber thermoplastic laminates, which this work aims to address.

Assessing self-healing abilities requires a thorough examination of damage mechanisms at various scales [34]. Traditional methods for evaluating macroscopic damage, such as bending, fracture toughness, or impact tests, often lead to catastrophic failures, including reinforcement rupture. Unfortunately, this type of damage cannot be repaired by a self-healing matrix, and the restored composite's properties fall short of the original properties. In essence, applying thermal repair to a composite with damaged reinforcement is neither an effective way to utilize the self-healing potential of the matrix nor a practical method for assessing healing efficiency. Other techniques allow for the introduction of microdamage concentrated in the matrix or at the interface/interlamina. Our recent work on thermoplastic self-healing discontinuous-fiber composites [33] involved the use of fatigue testing to insert controlled microdamage. Another test often employed to introduce microdamage to laminates is the short-beam shear (SBS) test, which specifically introduces interlaminar damage. The investigation of self-healing using SBS test has been reported many times in the literature for laminates with an epoxy matrix [7,17–19,35,36], and sometimes with a vitrimeric

[37] or a Diels-Alder [21] matrix, but never with a thermoplastic one.

Hence, the present study investigates the self-healing capabilities of long carbon fiber-reinforced PA6 based thermoplastic laminates produced through film stacking and hot pressing. This study focuses on evaluating the mechanical properties and repair performance of laminates produced with an optimized self-healing blend (PA6/30 wt% COC/5 wt% E-GMA) in comparison with reference laminates containing a PA6 matrix. The healing efficiency is assessed by determining the interlaminar shear strength (ILSS) by the SBS test before and after thermal mending, and a comprehensive microstructural analysis provides insights into the healing mechanisms operative in laminated structures. This work represents the first systematic investigation of intrinsic self-healing behavior in continuous carbon fiber thermoplastic laminates and aims to establish a foundation for advanced multifunctional structural composites with autonomous repair capabilities.

2. Materials and methods

2.1. Materials

The materials employed in this work were polyamide 6 (PA6, Radilon S 35/10, Radici Group, Bergamo, Italy) as the polymer matrix, cyclic olefinic copolymer (COC, TOPAS 6013, TOPAS Advanced Polymers, Frankfurt-Höchst, Germany) as the healing agent, poly(ethylene-co-glycidyl methacrylate) (E-GMA, Merck KGaA, Darmstadt, Germany) as the compatibilizer, and bidirectional carbon fiber fabric (GG 200P, G. Angeloni Srl, Venice, Italy) as the reinforcement. The PA6 grade was specifically selected for its excellent processability in terms of melt filmability and good thermal stability up to 300 °C. The COC healing agent is characterized by a glass transition temperature (T_g) of 65 °C and a density of 1.02 g/cm^3, enabling thermal activation for self-healing at moderate temperatures. The E-GMA compatibilizer, containing 6.5–9.0 wt% glycidyl methacrylate groups, was employed based on previous optimization studies of our group [38] to enhance interfacial adhesion between the PA6 matrix and COC domains. The bidirectional carbon fiber fabric featured an areal weight of 192 g/m^2 with individual fiber diameters of 7 μm and a polyamide-compatible sizing to promote matrix-fiber adhesion. All materials were dried prior to processing according to the suppliers' recommendations to prevent hydrolytic degradation and ensure optimal processing conditions.

2.2. Sample preparation

Sample preparation was divided into three sequential steps: (i) preparation of self-healing blends, (ii) preparation of matrix thin films, and (iii) preparation of composites through film stacking and hot pressing. All processing temperatures and conditions were carefully selected to remain well below the degradation temperatures of the constituents (>400 °C for COC, >350 °C for PA6) while ensuring adequate melt flow, as validated through extensive rheological and thermal characterization in our previous work [30,32,33].

Preparation of the self-healing blends.

Thermoplastic self-healing blends were prepared using melt compounding. Prior to processing, the PA6 granules were dried at 80 °C for 12 h in a vacuum oven, whereas the COC and E-GMA pellets were dried at 50 °C for 12 h in a ventilated oven. The blends were prepared using a Thermo Haake Rheomix 600 internal mixer equipped with counter-rotating rotors operating at 60 rpm. Initially, PA6 and COC were melt-compounded at a fixed weight ratio of 70/30 at a temperature of 230 °C for 1 min. Subsequently, E-GMA compatibilizer was added at a concentration of 5 wt%, and the mixture was processed for a total time of 6 min. The PA6/COC ratio was selected based on previous studies demonstrating optimal self-healing properties at this composition, while an E-GMA content of 5 wt% was determined as the best concentration for achieving a good balance between processability and self-healing efficiency [38]. After compounding, the obtained blends were pelletized using a Piovan RN166/1 grinder equipped with a 3-mm sieve for subsequent film extrusion.

2.2.1. Preparation of thin films

Thin polymeric films were prepared using a single-screw extruder equipped with a flat die system. The dried pellets of neat PA6 and the self-healing blend were processed through a Collin Teach-Line E20T single-screw extruder (Collin GmbH, Ebersberg, Germany) equipped with a Chill-Roll and a calender CR 72 T. Two different thermal profiles were employed to accommodate the different processability characteristics of the materials. For the neat PA6 films, the temperature profile from hopper to die was set at 225 °C – 235 °C – 245 °C – 225 °C – 215 °C with a screw speed of 40 rpm. For the self-healing blend films, a modified thermal profile of 225 °C – 230 °C – 235 °C – 230 °C – 225 °C was applied with a screw speed of 55 rpm. Different processing parameters were necessary due to the altered rheological properties of the compatibilized blend compared to neat PA6, as observed in previous studies by our group [33,38]. The extruded films, with a thickness of 150 μm, were cooled using a chill-roll system and wound for subsequent composite preparation.

2.2.2. Preparation of the composites

The final composite preparation involved film stacking and hot pressing (Fig. 1). The thermoplastic thin films were alternately stacked with bidirectional carbon fiber fabrics to achieve the desired laminate configuration. The stacking sequence was designed to ensure a uniform distribution of the matrix throughout the composite structure. The stacked assemblies were then consolidated using a two-step hot-pressing procedure. First, the composite stacks were placed in a hot press at 240 °C for 5 min without applying pressure to allow complete melting and flow of the thermoplastic matrix. Subsequently, the pressure was gradually increased to 2 MPa and maintained for 10 min to ensure complete fiber impregnation and void limitation. Consolidation was completed by cooling the composites under maintained pressure to prevent distortion and ensure dimensional stability. This film stacking and hot-pressing approach enabled the production of high-quality thermoplastic composites with a controlled fiber volume fraction and minimized void content, suitable for mechanical characterization and self-healing evaluation. Laminates of two different thicknesses were produced, i.e., (i) the "thin" laminates, with an average thickness of 2.0 mm, denominated as 'PA6CF_TF' or 'PA6COCCF_TF', are those made of 11 polymer films and 10 CF laminates and used for the tensile tests and the flexural tests, and (ii) the "thick" laminates, with an average thickness of 3.4 mm, denominated as 'PA6CF_S' or 'PA6COCCF_S', are those made of 17 polymer films and 16 CF laminates and used for the short beam shear (SBS) tests. This was done to be able to prepare specimens with geometries in agreement with the relevant ASTM standards, as reported in the Characterization section.

2.3. Characterization

2.3.1. Microstructural analysis

Light microscopy (LM) was performed on the polished cross sections and fractured surfaces using a CH 9435 Heerbrugg optical microscope (Heerbrugg, Switzerland). Specimens were embedded in epoxy resin, cured for 24 h at room temperature, and subsequently polished using a Struers LaboPol-5 system with sequential silicon carbide papers (240, 800, 1200, and 4000 grit), followed by polishing cloths (3 μm and 1 μm). ImageJ® software was used for dimensional analysis and morphological evaluation.

2.3.2. Thermal analysis

Thermogravimetric analysis (TGA) was conducted using a TA Instruments Q5000 IR thermobalance with a heating rate of 10 °C/min up to 700 °C under a nitrogen atmosphere (10 ml/min). TGA enabled the determination of the temperatures corresponding to a mass loss of 1 wt%

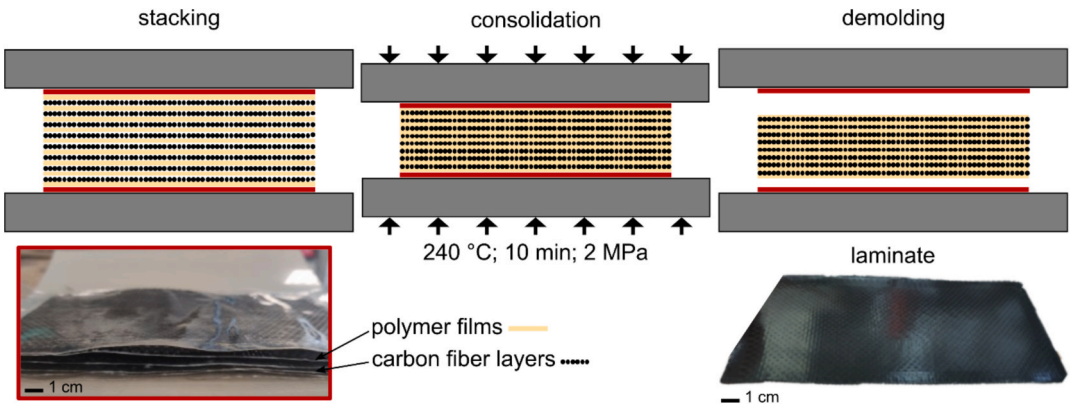

Fig. 1. Schematic representation of the film stacking and hot pressing process utilized for the production of the thermoplastic composites.

and 5 wt% ($T_{1\%}$, $T_{5\%}$), indicative of the first degradation steps, the temperature corresponding to the maximum degradation kinetics, taken as the peak of the derivative thermogravimetry (DTG) curve (T_d), and the residual mass after the test (m_r), from which the fiber weight fraction for theoretical density calculations was drawn.

2.3.3. Density and void content

The experimental density (ρ_{exp}) was measured using a Micrometrics AccuPyc 1330 helium pycnometer. Void content (v_v [vol%]) was calculated according to Eq. (1),

$$v_v = \frac{\rho_{th} - \rho_{exp}}{\rho_{th}} \bullet 100 \quad (1)$$

where ρ_{th} is the theoretical density calculated from the constituent densities, measured with the same technique, and fiber weight fractions determined by TGA.

2.3.4. Mechanical testing

Tensile tests were performed according to ASTM D3039 on rectangular specimens (120 × 10 mm^2) cut from laminates using a diamond saw. The tests were conducted using an Instron 5969 universal testing machine (Norwood, MA, USA) with composite tabs to prevent grip damage. The elastic modulus (E) was measured at 0.25 mm/min crosshead speed using an Instron 2620–601 extensometer with a gauge length of 12.5 mm, calculated as the secant modulus between strain values of 0.05 % and 0.25 %. The ultimate properties (ultimate tensile strength, UTS, and strain at break, ε_b) were determined at a crosshead speed of 1 mm/min. A minimum of six specimens were tested for each composition.

Flexural tests followed ASTM D790 in a three-point bending configuration using the same universal testing machine. Specimens with nominal dimensions of 80 × 13 × 2 mm^3 were tested with a support span-to-thickness ratio of 32:1. The crosshead speed was calculated according to standard requirements to maintain a constant outer fiber strain rate of 0.01 mm/mm/min. The test allowed determining the flexural modulus (E_f), flexural strength (σ_{fM}), and flexural strain at break (ε_{fb}). The crosshead displacement was used to calculate strain/deflection.

Short beam shear (SBS) tests were performed according to ASTM D2344 to evaluate the interlaminar shear strength (ILSS). The specimen dimensions were determined based on the laminate thickness following the Standard requirements (width = 2 × h, span = 4 × h, length = 6 × h, where h is the specimen thickness). Tests were conducted at a crosshead speed of 1 mm/min with at least six specimens per composition. As reported in the standard, the test was performed until a load drop-off of 30 % or until the head travel exceeded the specimen nominal thickness. ILSS was calculated according to Eq. (2),

$$ILSS = \frac{3P_{max}}{4bh} \bullet 100 \quad (2)$$

where P_{max} is the maximum load, b is the width, and h the thickness of the specimen. The crosshead displacement was used to calculate strain/deflection.

2.3.5. Self-healing evaluation

The self-healing properties were assessed via thermal mending of the SBS-tested specimens. Healing was performed in a Carver hot press at 160 °C for 1 h under 0.5 MPa pressure, with cooling to room temperature performed under pressure. This temperature was selected based on previous optimization studies [38], as it exceeds the T_g of COC and ensures sufficient macromolecular mobility for healing agent flow. The healing efficiency (HE) was quantified as the ratio between the ILSS value measured on the repaired sample and that measured on the virgin one.

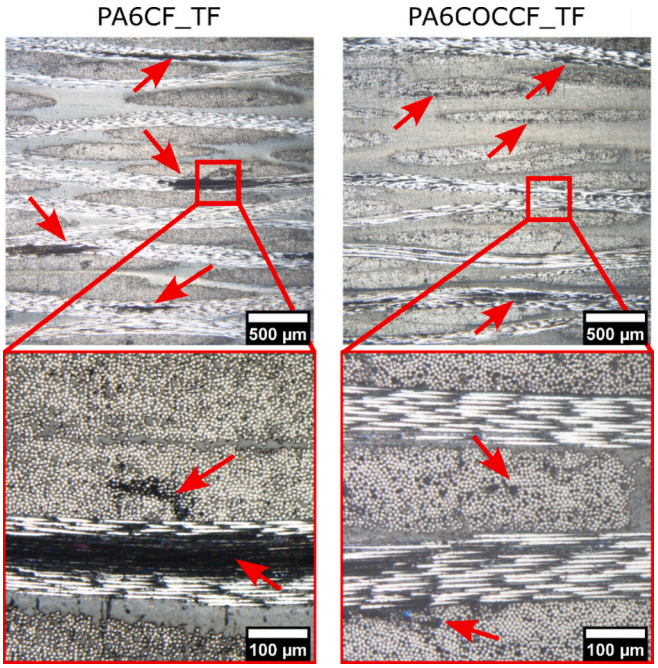

Fig. 2. Light microscopy micrographs of polished PA6CF_TF and PA6COCCF_TF composites at different magnifications. Arrows indicate areas of incomplete impregnation.

3. Results and discussion

Fig. 2 shows the microstructures of the PA6CF_TF and PA6COCCF_TF laminates, revealing the characteristic 0/90° pattern of the bidirectional carbon fiber fabric. Both laminates exhibit matrix-rich regions in the interlaminar areas, as commonly found in composites prepared via film stacking. Such interlaminar regions appear qualitatively thicker for the self-healing composite based on microscopic examination, likely due to the higher matrix viscosity [33], though the thickness varies considerably across the laminate due to the fabric waviness. Black spots indicate areas of poor fiber impregnation, particularly in the inner regions of the carbon fiber tows (intralaminar zones). This impregnation challenge is typical for thermoplastic matrices, as highlighted in the literature [39], particularly for high-viscosity matrices. However, the composites with the self-healing blend, more viscous than neat PA6 [33], do not show worse impregnation, and the number and extent of areas of poor impregnation are comparable to those of the PA6CF composite.

The porosity and incomplete fiber impregnation observed in Fig. 2 are reflected in the discrepancy between the theoretical and experimental densities and the consequent presence of voids (Table 1). All laminates exhibit similar void contents, ranging from 2.3 vol% to 4.4 vol %. Interestingly, the higher viscosity of the self-healing blend did not significantly increase the void content compared to neat PA6. In fact, for both thicknesses, the void volume fractions of the composites with the PA6COC matrix are slightly lower than those of the neat PA6CF laminates. This result may stem from the enhanced fiber–matrix compatibility provided by E-GMA reducing interfacial tension and improving wetting, combined with the broader processing window and more stable flow behavior of the PA6/COC blend throughout the consolidation temperature range, which together facilitate void evacuation despite the higher bulk viscosity. Although the investigation of the porosity formation and elimination is outside the scope of this work, the low and comparable porosity across all the produced laminates suggests that film stacking was adequate for both matrix systems, and confirms the qualitative observations shown in Fig. 2. Moreover, the self-healing matrix yields composites with slightly lower fiber weight and volume fractions, for both the TF and S laminates. This is likely due to the higher viscosity of the PA6COC matrix compared to that of neat PA6, which results in thicker interlaminar regions, as qualitatively observed in Fig. 2. Hence, while the process employed in this work demonstrates feasibility, optimization is needed for industrial implementation. Key areas for improvement include fine-tuning processing parameters (temperature profile, pressure ramp rate, dwell time) to further decrease void concentration and achieve more consistent fiber volume fractions and thickness of the interlaminar region. This will be needed to overcome the viscosity-related limitations while maintaining self-healing functionality in a future industrial scale up.

Fig. 3 shows the TGA curves for all the prepared laminates, and the key results are summarized in Table 2. The significant m_r values at 700 °C (58–72 wt%) correspond largely to the carbon fiber content and were used for theoretical density calculations. All laminates exhibit similar thermal degradation onset temperatures ($T_{1\%}$, $T_{5\%}$) and maximum degradation temperature (T_d), indicating that the self-healing composites maintain a thermal stability comparable to that of neat

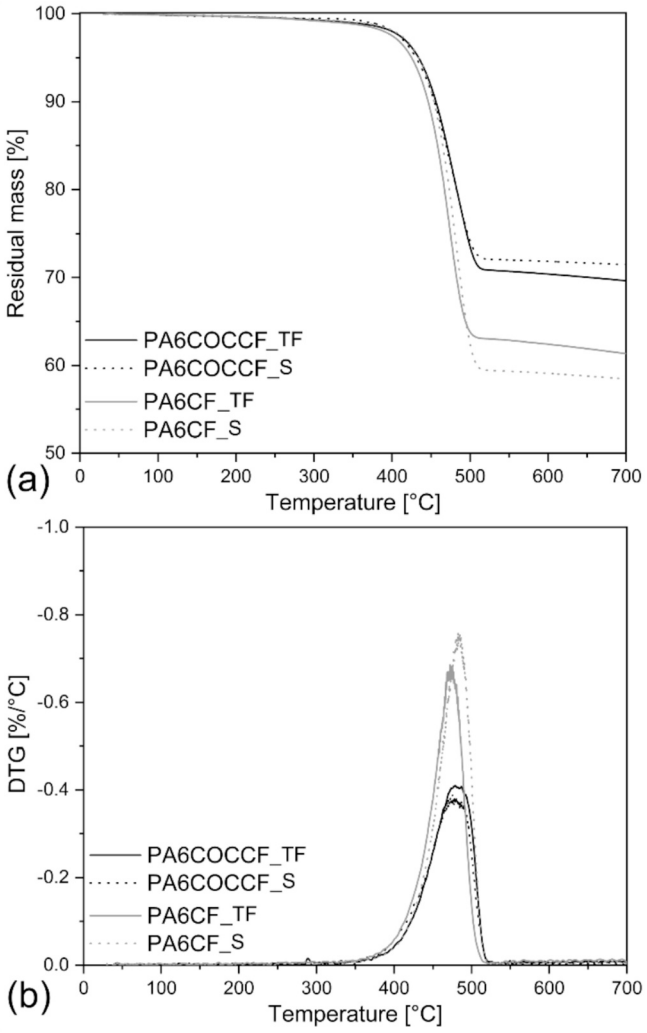

Fig. 3. TGA thermograms of the prepared composites. (a) Residual mass and (b) derivative of mass loss (DTG) as a function of temperature.

Table 2
Results of TGA tests on the prepared composites.

Sample	$T_{1\%}$ [°C]	$T_{5\%}$ [°C]	T_d [°C]	m_r [%]
PA6CF_TF	347.3	434.2	479.2	69.6
PA6CF_S	372.8	430.7	475.2	71.5
PA6COCCF_TF	332.0	425.0	472.2	61.3
PA6COCCF_S	356.3	434.2	484.3	58.5

$T_{1\%}$, $T_{5\%}$ = temperatures corresponding to a mass loss of 1 wt% or 5 wt%; T_d = degradation temperature; m_r = residual mass after the test.

Table 1
Density and relative composition of the prepared composites.

Sample	ρ_{exp} [g/cm^3]	ρ_{th} [g/cm^3]	w_m [wt%]	w_{CF} [wt%]	v_m [vol%]	v_{CF} [vol%]	v_v [vol%]
PA6CF_TF	1.41 ± 0.01	1.48	26.4	73.6	38.6	61.4	4.4 ± 0.1
PA6CF_S	1.44 ± 0.01	1.50	24.4	75.6	36.1	63.9	3.6 ± 0.1
PA6COCCF_TF	1.40 ± 0.01	1.44	35.2	64.8	47.3	52.7	2.7 ± 0.1
PA6COCCF_S	1.38 ± 0.01	1.42	38.2	61.8	50.6	49.4	2.3 ± 0.1

ρ_{exp} = experimental density; ρ_{th} = theoretical density; w_m = matrix weight fraction; w_{CF} = fiber weight fraction; v_m = matrix volume fraction; v_{CF} = carbon fiber volume fraction; v_v = void volume fraction.

PA6CF laminates. The similar TGA patterns also confirm that no thermal degradation occurred during film processing or laminate consolidation, validating the selected processing conditions and demonstrating the thermal compatibility of the PA6/COC/E-GMA system with carbon fiber reinforcement.

The mechanical properties of the prepared "TF" thermoplastic laminates were assessed through tensile and flexural tests. Representative tensile stress–strain curves are reported in Fig. 4a for both PA6CF and PA6COCCF, while Table 3 reports the most important results. The shape of the initial part of the stress–strain curve (toe region) is influenced by the slight compliance of the grips inside the testing machine. PA6COCCF samples report a higher elastic modulus, stress at break, and strain at break compared to neat PA6GF. The superior mechanical performance of PA6COCCF compared to PA6CF can be attributed to the lower void content (Table 1), improved fiber wettability, and potentially enhanced compatibility between the fiber sizing agent and the PA6COC matrix through E-GMA reactions [33], although further investigation is needed to fully clarify this point.

The improved wetting and interfacial interaction in the PA6COCCF composites are also observable from the LM micrographs of the fracture surfaces shown in Fig. 4(b-e). The PA6CF micrographs reveal delamination failure with visible unbound carbon fibers, confirming the wetting issues previously identified. In contrast, PA6COCCF demonstrates effective matrix infiltration with characteristic fiber rupture, indicating improved fiber–matrix interaction [40].

The results of the flexural tests are shown in Fig. 5, which exhibits representative flexural stress–strain curves for both PA6CF and PA6COCCF, while Table 3 reports the most important results. The fracture analysis of each specimen was conducted in accordance with ASTM D7264 standards, enabling the identification of various fracture mechanisms. The fracture of PA6CF is brittle, and the specimens fail almost instantaneously at the maximum load, with the load dropping almost to zero in a single damaging event, whereas PA6COCCF reports a progressive fracture propagation mode. A decrease in flexural strength is observed for the PA6COCCF laminates, showing a reduction of 17 % compared to the PA6CF composites. This reduction can be attributed to the slightly lower fiber volume fraction, but also to the diminished mechanical properties of the self-healing matrix [33,38], which leads to a premature failure of the matrix-rich interlaminar region. A similar trend is observed in the strain at break, which decreases from 1.5 % for the PA6CF composite to 1.0 % for the self-healing composite. Hence, while E-GMA compatibilization improves fiber–matrix adhesion benefiting tensile properties, the inherently lower stiffness and strength of the PA6COC matrix becomes the limiting factor in flexural loading where matrix properties play a more critical role in resisting compressive stresses, especially with a thicker interlaminar region.

The diminished flexural strength of the PA6COCCF laminate compared to that of PA6CF can be better understood by delving deeper into the damaging mechanisms. The neat PA6CF laminate exhibits two subsequent fracture events: the first, in the top-central portion of the specimen, below the loading nose, due to bucking of the first lamina, and the second, in the bottom-central portion of the specimen, due to the tensile stress. The self-healing PA6COCCF laminate also experiences buckling-derived damage, but the subsequent damage mechanism is related more to a sequence of delamination and matrix-breaking steps instead of a single, sudden, tensile-driven event. Such differences are appreciable both from the representative stress–strain curves (Fig. 5a) and from the LM micrographs of the polished lateral surfaces of the top-central and bottom-central portions of the two specimens after the flexural test (Fig. 5b-e).

For the PA6CF specimens (Fig. 5b-c), the top-central region exhibits multiple matrix and fiber cracks, along with characteristic buckling at the loading point that caused severe delamination in the first lamina. The bottom-central region reveals extensive damage with both the matrix and fibers completely fractured, thus explaining the drastic stress drop observed in the stress–strain curve (Fig. 5a). In contrast, in the shown PA6COCCF specimen (Fig. 5d-e), the top-central region is characterized by only one fiber fracture but multiple matrix cracks, with buckling-induced delamination extending across several laminae rather than being confined to the first layer, as in PA6CF. This multilaminar delamination provides additional energy dissipation mechanisms. Importantly, the fiber integrity is maintained until a very advanced damage stage, because damage concentrates mostly in the matrix. This is favorable because only the matrix can self-heal. The bottom-central

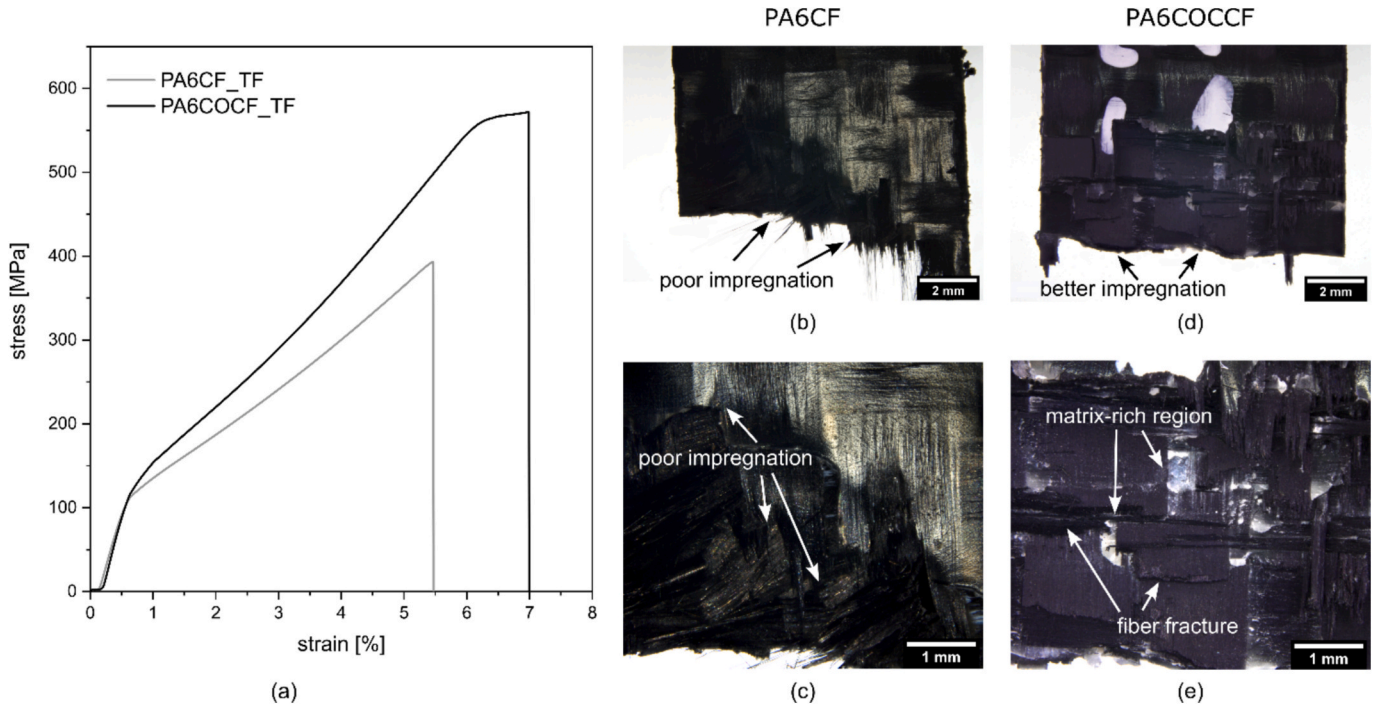

Fig. 4. Representative tensile stress–strain curves of PA6CF_TF and PA6COCCF_TF composites; (b,c) LM micrographs of the fracture surfaces of PA6CF_TF after the tensile tests; (d,e) LM micrographs of the fracture surfaces of PA6COCCF_TF specimens after the tensile tests.

Table 3
Results of tensile and flexural tests on the prepared composites (average value ± standard deviation).

Sample	E[GPa]	UTS[MPa]	ε_b[%]	E_f[GPa]	σ_{fM}[MPa]	ε_{fb}[%]
PA6CF_TF	55 ± 3	374 ± 54	4.9 ± 0.9	46 ± 4	599 ± 66	1.5 ± 0.2
PA6COCCF_TF	62 ± 2	534 ± 28	6.0 ± 0.9	48 ± 5	498 ± 48	1.0 ± 0.3

E = tensile elastic modulus; UTS = ultimate tensile strength; ε_b= tensile strain at break; E_f = flexural modulus; σ_{fM} = flexural strength; ε_{fb}= flexural strain at break.

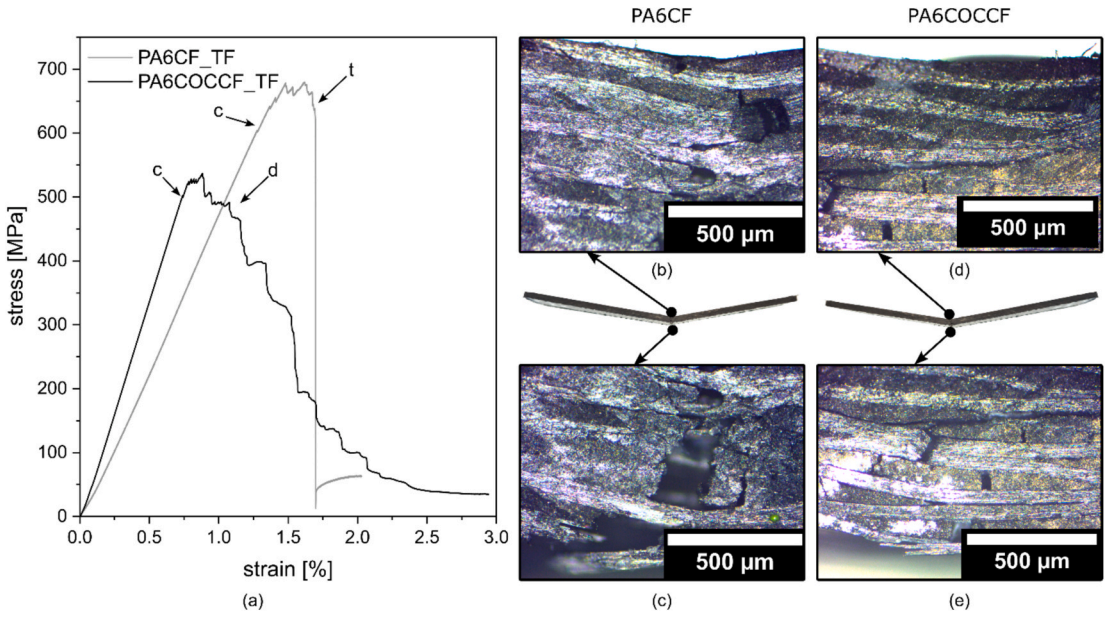

Fig. 5. (a) Representative stress–strain curves from flexural tests of PA6CF_TF and PA6COCCF_TF composites. c = compression-related damage and buckling of the first lamina; t = tensile-related damage; d = delamination. (b,c) LM micrographs of the polished fracture surface of PA6CF_TF after the flexural tests. (d,e) LM micrographs of the polished fracture surface of PA6COCCF_TF after the flexural tests.

portion of the specimen in PA6COCCF is notably less damaged than that in PA6CF, with crack propagation primarily through the matrix. This behavior explains the progressive stress drop after the maximum load in the PA6COCCF stress–strain curve (Fig. 5a), in contrast with the sudden, fiber-driven failure of PA6CF.

Hence, a significant decrease in the ultimate flexural properties is observed for the self-healing laminate due to a decrease in the matrix properties. However, such a decrease triggers alternative mechanisms that concentrate the damage in the matrix in the early damaging stages, thereby preserving the fibers and facilitating property recovery in the self-healing step, since the matrix is the only phase that can repair itself during healing. Such matrix-related damaging mechanisms may be unorthodox and surely not often pursued in continuous-fiber laminates, but may be one of the keys for designing high-performance composites that are repairable and thus more reliable and sustainable. In other words, this self-healing capability is most valuable as a damage-tolerant design feature that extends component lifetime by repeatedly repairing matrix microdamage, preventing its accumulation into critical defects. This approach is particularly relevant for applications involving cyclic loading where matrix fatigue damage accumulates over time, as demonstrated in our previous work on discontinuous fiber composites [33].

To benefit from this design perspective and avoid excessive impairment of the absolute properties, one parameter that can be further optimized is the thickness of the interlaminar region. For example, reducing the thickness of the matrix films would reduce matrix accumulation in the interlaminar region, which would improve the fiber distribution and increase the fiber volume fraction. However, this may promote a transition of the damage mode from mostly interlaminar to intralaminar, which could be difficult to repair because of the more limited presence and flowing ability of the healing agent within the fiber bundles. This issue could be addressed in the future by establishing the minimum interlaminar thickness that preserves the desired failure mechanism while optimizing mechanical properties or by promoting a more homogeneous and finer distribution of the healing agent domains, to address all the possible matrix-related damage modes.

Finally, SBS tests were performed to investigate the interlaminar properties of the prepared laminates and to concentrate the damage in the matrix-dominated interlaminar region, to exploit the healing mechanisms of the matrix during thermal mending. In fact, the extensive damage introduced during SBS testing primarily consists of matrix cracking, fiber–matrix delamination, and plasticization while preserving fiber integrity, which is fundamental for achieving a high healing efficiency in self-healing composites. Given the damaging mechanism occurring mostly by delamination (although some plasticization was also observed), the maximum load acquired during the test could be used to calculate the ILSS, according to Eq. (2). The ILSS values obtained for PA6CF and PA6COCCF (Fig. 6a) are comparable and consistent with the literature values for similar systems [41].

The tested specimens were subsequently thermally mended by placing them in a hot press under 0.5 MPa pressure at 160 °C for 1 h and retested to determine the ILSS after healing. The healing efficiency was calculated as the ratio of the ILSS of the healed specimen to that of the virgin specimen. The SBS test induced permanent deformation in all samples, and the pressure applied during healing effectively flattened all the specimens. However, as expected, PA6CF laminates cannot recover mechanical properties upon thermal treatment, and the *HE* is only 14 ± 5 %, mainly attributed to carbon fiber interlocking during healing. In contrast, PA6COCCF laminates demonstrate complete damage restoration with a *HE* of 104 ± 7 %, indicating that the SBS properties of the

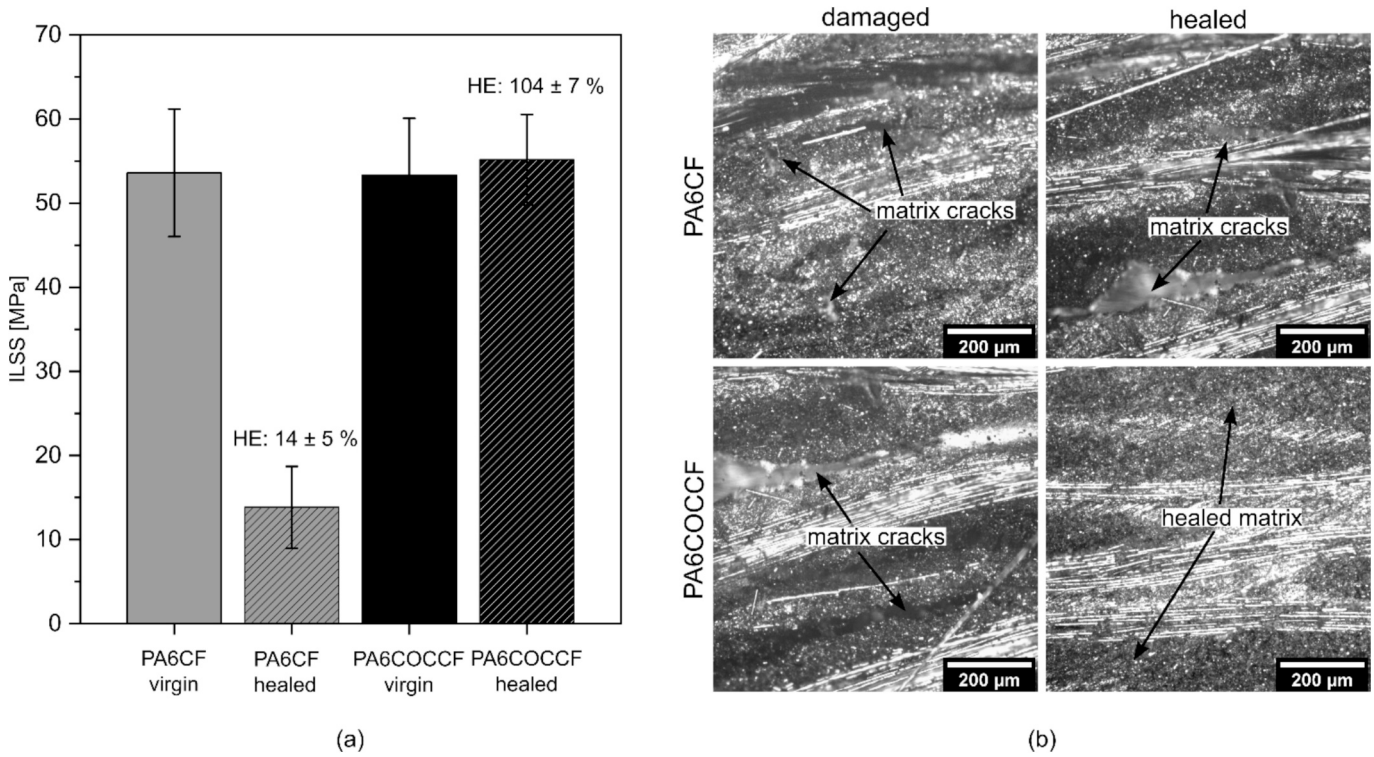

Fig. 6. (a) Results of SBS tests (values of interlaminar shear strength, ILSS) of the prepared laminates before and after thermal mending and values of healing efficiency (HE); (b) LM micrographs of the PA6CF_S and PA6COCCF_S laminates tested for the determination of the ILSS, before and after thermal mending.

damaged and healed composites are not significantly different from those of the virgin ones.

Fig. 6b shows LM micrographs of the lateral surfaces of the prepared composites before and after thermal mending. It should be noted that the specimens were polished prior to SBS testing to preserve the fractured/healed surfaces for analysis. PA6CF specimens exhibit multiple matrix cracks and fiber ruptures, with the bottom laminae torn apart due to high tensile loads and extensive lateral delamination. After thermal treatment, PA6CF shows no noticeable damage recovery, with matrix cracks remaining visible. Conversely, PA6COCCF specimens display extensive matrix cracks and delamination before healing, but after thermal mending, the compatibilized COC flows and fills microcracks and delaminated regions. The post-healing micrographs show the complete absence of matrix cracks or delamination, providing clear evidence for the exceptional ILSS recovery observed in the self-healing laminates.

4. Conclusions

This study demonstrated the successful preparation of self-healing thermoplastic composite samples through film stacking and hot pressing of PA6/COC/E-GMA blends with bidirectional carbon fiber fabrics. Despite the higher viscosity of the self-healing matrix leading to some impregnation challenges, self-healing composites demonstrated lower porosity (2.3–2.7 vol%) than the neat ones (3.6–4.4 vol%).

Mechanical characterization revealed that PA6COCCF laminates exhibited superior tensile properties compared to PA6CF, with higher *UTS* and strain at break, attributed to improved fiber–matrix interaction through E-GMA compatibilization. On the other hand, the ultimate flexural properties showed a slight decrease for the self-healing system due to the lower fiber volume fraction and the decreased mechanical properties of the COC-containing matrix compared to neat PA6, although the values remained appropriate for structural use. Both systems demonstrated similar thermal stability and comparable ILSS values.

The most significant finding is the exceptional self-healing capability of the PA6COCCF system after creating damage through the SBS test. While PA6CF laminates showed minimal recovery (*HE* = 14 %), PA6COCCF achieved complete damage restoration after thermal treatment at 160 °C, indicating that the ILSS of the repaired composites was not significantly different from that of the neat laminates. Microstructural analysis confirmed that the compatibilized COC effectively flowed and filled matrix cracks and delaminated regions during healing, eliminating visible damage. The SBS test proved particularly suitable for evaluating self-healing performance, as it inflicts damage primarily to the matrix while preserving fiber integrity, which is essential for thermoplastic self-healing systems that can only repair matrix-related damage.

These results demonstrate that a compatibilized PA6/COC self-healing matrix could be successfully integrated with continuous carbon fiber reinforcement with no significant impairment in mechanical performance, while providing outstanding damage recovery capabilities. Importantly, the healing process at 160 °C, being over 60 °C below the PA6 melting temperature (220 °C), enables in-situ repair while maintaining dimensional stability and structural integrity – a critical advantage over conventional thermoplastic welding that would require processing well above 220 °C with associated risks of distortion and degradation. Further optimization could focus on reducing the thickness of the matrix films to achieve thinner interlaminar regions to try and limit the observed decrease in flexural properties. The developed composites show significant potential for structural applications where damage tolerance and extended service life are critical, particularly in components subjected to matrix-dominated failure modes, such as delamination and matrix cracking.

CRediT authorship contribution statement

Davide Perin: Writing – review & editing, Visualization, Validation, Methodology, Investigation, Data curation, Conceptualization. **Giulia Fredi:** Writing – review & editing, Writing – original draft,

Visualization, Validation, Formal analysis. **Pietro Russo:** Writing – review & editing, Methodology, Investigation, Conceptualization. **Alessandro Pegoretti:** Writing – review & editing, Supervision, Resources, Project administration, Funding acquisition, Conceptualization. **Andrea Dorigato:** Writing – review & editing, Supervision, Resources, Project administration, Methodology, Funding acquisition, Conceptualization.

Funding

Funded by the European Union - Next Generation EU - PNRR, Mission 4 Component 2, Investment 1.3 - PE MICS Spoke 5 - LOLIMAR Project (PE00000004, CUP D43C22003120001).

Declaration of competing interest

The authors declare that they have no known competing financial interests or personal relationships that could have appeared to influence the work reported in this paper.

Data availability

Data will be made available on request.

References

[1] Arora S, Chitkara R, Dhangar AS, Dubey D, Kumar R, Gupta A. A review of fatigue behavior of FRP composites. Mater Today: Proc 2022;64:1272–5. https://doi.org/10.1016/j.matpr.2022.04.034.
[2] Zhang ZP, Rong MZ, Zhang MQ. Self-healable functional polymers and polymer-based composites. Prog Polym Sci 2023;144. https://doi.org/10.1016/j.progpolymsci.2023.101724.
[3] Cioffi MOH, Bomfim ASC, Ambrogi V, Advani SG. A review on self-healing polymers and polymer composites for structural applications. Polym Compos 2022;43(11):7643–68. https://doi.org/10.1002/pc.26887.
[4] Utrera-Barrios S, Verdejo R, López-Manchado MA, Hernández Santana M. Evolution of self-healing elastomers, from extrinsic to combined intrinsic mechanisms: a review. Mater Horizons 2020;7(11):2882–902. https://doi.org/10.1039/D0MH00535E.
[5] Malekkhouyan R, Neisiany RE, Khorasani SN, Das O, Berto F, Ramakrishna S. The influence of size and healing content on the performance of extrinsic self-healing coatings. J Appl Polym Sci 2021;138(10):49964. https://doi.org/10.1002/app.49964.
[6] Brown EN, White SR, Sottos NR. Microcapsule induced toughening in a self-healing polymer composite. J Mater Sci 2004;39:1703–10.
[7] Nassho Y, Sanada K. Microstructure optimizations for improving interlaminar shear strength and self-healing efficiency of spread carbon fiber/epoxy laminates containing microcapsules. J Compos Mater 2020;55(1):27–38. https://doi.org/10.1177/0021998320943941.
[8] Wang J, Tang J, Chen D, Xing S, Liu X, Hao J. Intrinsic and extrinsic self-healing fiber-reinforced polymer composites: a review. Polym Compos 2023;44(10):6304–23. https://doi.org/10.1002/pc.27623.
[9] Benazzo F, Rigamonti D, Sala G, Grande AM. A critical appraisal of fracture mechanics methods for self-healing and healable composites characterization. Compos A Appl Sci Manuf 2023;167. https://doi.org/10.1016/j.compositesa.2023.107450.
[10] Turicek JS, Snyder AD, Nakshatrala KB, Patrick JF. Topological effects of 3D-printed copolymer interlayers on toughening and in situ self-healing in laminated fiber-composites. Compos Sci Technol 2023;240. https://doi.org/10.1016/j.compscitech.2023.110073.
[11] Simonini L, Kakkonen M, Dsouza R, Kanerva M, Mahmood H, Dorigato A, et al. Tailoring the interfacial properties of glass fiber-epoxy microcomposites through the development of a self-healing poly(ϵ-caprolactone) coating. Compos Sci Technol 2025;261:110991. https://doi.org/10.1016/j.compscitech.2024.110991.
[12] Simonini L, Mahmood H, Dorigato A, Pegoretti A. Evaluation of self-healing capability of a polycaprolactone interphase in epoxy/glass composites. Compos A Appl Sci Manuf 2023;169:107539. https://doi.org/10.1016/j.compositesa.2023.107539.
[13] Varley RJ, Craze DA, Mouritz AP, Wang CH. Thermoplastic healing in epoxy networks: exploring performance and mechanism of alternative healing agents. Macromol Mater Eng 2013;298(11):1232–42. https://doi.org/10.1002/mame.201200394.
[14] Jones AR, Watkins CA, White SR, Sottos NR. Self-healing thermoplastic-toughened epoxy. Polymer 2015;74:254–61. https://doi.org/10.1016/j.polymer.2015.07.028.
[15] Yang T, Du Y, Li ZM, Wang CH. Mechanical properties of self-healing carbon fiber-epoxy composite stitched with mendable polymer fiber. Polymers & Polymer Composites 2014;22(3):329–36.
[16] Wang K, Xiao H, Li M, Luan Y, Cai H. The interlaminar toughening and low-temperature repeated self-healing properties of CF/BMI composites. Polym Compos 2025. https://doi.org/10.1002/pc.29718.
[17] Cai H, Li M, Gan Y, Xiao H, Wang K, Luan Y. Toughening and self-healing of carbon fiber/epoxy composites interleaved with meltable/non-meltable polyamide nanofiber veils. Polym Compos 2025. https://doi.org/10.1002/pc.30049.
[18] Chen B, Cai H, Mao C, Gan Y, Wei Y. Toughening and rapid self-healing for carbon fiber/epoxy composites based on electrospinning thermoplastic polyamide nanofiber. Polym Compos 2022;43(5):3124–35. https://doi.org/10.1002/pc.26605.
[19] Wang CH, Sidhu K, Yang T, Zhang J, Shanks R. Interlayer self-healing and toughening of carbon fibre/epoxy composites using copolymer films. Compos A Appl Sci Manuf 2012;43(3):512–8. https://doi.org/10.1016/j.compositesa.2011.11.020.
[20] Karger-Kocsis J. Self-healing properties of epoxy resins with poly(ε-caprolactone) healing agent. Polym Bull 2016;73(11):3081–93. https://doi.org/10.1007/s00289-016-1642-2.
[21] Heo Y, Sodano HA. Thermally responsive self-healing composites with continuous carbon fiber reinforcement. Compos Sci Technol 2015;118:244–50. https://doi.org/10.1016/j.compscitech.2015.08.015.
[22] Cescato R, Rigotti D, Mahmood H, Dorigato A, Pegoretti A. Thermal mending of electroactive carbon/epoxy laminates using a porous Poly(epsilon-caprolactone). Electrospun Mesh, Polymers (Basel) 2021;13(16). https://doi.org/10.3390/polym13162723.
[23] CostanZovi R, Mahmood H, Dorigato A, Fredi G, Pegoretti A. Cyclic olefin copolymer interleaves for thermally mendable carbon/epoxy laminates. Molecules 2020;25(22). https://doi.org/10.3390/molecules25225347.
[24] Mahmood H, Dorigato A, Pegoretti A. Thermal mending in novel epoxy/cyclic olefin copolymer blends. Express Polym Lett 2020;14(4):368–83. https://doi.org/10.3144/expresspolymlett.2020.31.
[25] Mahmood H, Dorigato A, Pegoretti A. Healable carbon fiber-reinforced epoxy/cyclic olefin copolymer composites. Materials (Basel) 2020;13(9). https://doi.org/10.3390/ma13092165.
[26] Aina AN, Rizal MAM, Rased MFA, Hassan SA, Ng LF, Rajeshkumar L, et al. Fiber-reinforced thermoplastic composites for future use in aircraft radomes: biomimetic design approaches and its performances. Fibers Polym 2024;25(12):4503–27. https://doi.org/10.1007/s12221-024-00776-1.
[27] Valentini M, De Almeida O, Kakkonen M, Kalinka G, Dorigato A, Kallio P, et al. Effect of fiber surface state on the thermomechanical and interfacial properties of in situ polymerized polyamide 6/basalt fiber composites. Compos A Appl Sci Manuf 2025;190:108681. https://doi.org/10.1016/j.compositesa.2024.108681.
[28] Pegoretti A. Towards sustainable structural composites: a review on the recycling of continuous-fiber-reinforced thermoplastics. Adv Ind Eng Polym Res 2021;4(2):105–15. https://doi.org/10.1016/j.aiepr.2021.03.001.
[29] Ma Z, Xu Z, Li Z, Chen S, Wu Y, Yan J. Improving the quality of resistance welded thermoplastic composite joints by applying ultrasonic. Compos B Eng 2024;277. https://doi.org/10.1016/j.compositesb.2024.111398.
[30] Perin D, Dorigato A, Pegoretti A. Thermoplastic self-healing polymer blends for structural composites: development of polyamide 6 and cyclic olefinic copolymer blends. J Appl Polym Sci 2023;140(16):e53751. https://doi.org/10.1002/app.53751.
[31] Perin D, Odorizzi G, Dorigato A, Pegoretti A. Development of polyamide 6 (PA6)/polycaprolactone (PCL) thermoplastic self-healing polymer blends for multifunctional structural composites. Appl Sci 2022;12(23):12357. https://doi.org/10.3390/app122312357.
[32] Perin D, Dorigato A, Pegoretti A. Compatibilization of polyamide 6/cyclic olefinic copolymer blends for the development of multifunctional thermoplastic composites with self-healing capability. Materials 2024;17(8):1880.
[33] Coser M, Perin D, Fredi G, Aliotta L, Gigante V, Lazzeri A, et al. Self-healing of polyamide 6/cyclic olefin copolymer/carbon fiber composites under quasi-static, impact, and fatigue conditions. Compos Sci Technol 2025;268. https://doi.org/10.1016/j.compscitech.2025.111213.
[34] Tsangouri E, Aggelis D, Van Hemelrijck D. Quantifying thermoset polymers healing efficiency: a systematic review of mechanical testing. Prog Polym Sci 2015;49–50:154–74. https://doi.org/10.1016/j.progpolymsci.2015.06.002.
[35] Neisiany RE, Lee JKY, Khorasani SN, Ramakrishna S. Self-healing and interfacially toughened carbon fibre-epoxy composites based on electrospun core–shell nanofibres. J Appl Polym Sci 2017;134(31). https://doi.org/10.1002/app.44956.
[36] Moll JL, Jin H, Mangun CL, White SR, Sottos NR. Self-sealing of mechanical damage in a fully cured structural composite. Compos Sci Technol 2013;79:15–20. https://doi.org/10.1016/j.compscitech.2013.02.006.
[37] Perrin H, Vaudemont R, Del Frari D, Verge P, Puchot L, Bodaghi M. On the cyclic delamination-healing capacity of vitrimer-based composite laminates. Compos A Appl Sci Manuf 2024;177. https://doi.org/10.1016/j.compositesa.2023.107899.
[38] Perin D, Rigotti D, Botta L, Dorigato A, Fredi G, Pegoretti A. Tuning the compatibilizer content and healing temperature in thermally mendable polyamide 6/cyclic olefin copolymer blends. Polymers 2025;17:280. https://doi.org/10.3390/polym17030280.
[39] Ma Y, Ueda M, Yokozeki T, Sugahara T, Yang Y, Hamada H. A comparative study of the mechanical properties and failure behavior of carbon fiber/epoxy and carbon

fiber/polyamide 6 unidirectional composites. Compos Struct 2017;160:89–99. https://doi.org/10.1016/j.compstruct.2016.10.037.
[40] Ning H, Lu N, Hassen AA, Chawla K, Selim M, Pillay S. A review of Long fibre thermoplastic (LFT) composites. Int Mater Rev 2020;65(3):164–88. https://doi.org/10.1080/09506608.2019.1585004.
[41] Prabhakaran RTD, Toftegaard H. Environmental effect on the mechanical properties of commingled-yarn-based carbon fibre/polyamide 6 composites. J Compos Mater 2014;48(21):2551–65. https://doi.org/10.1177/0021998313501012.